Neurobiology of Disease 110 (2018) 29–36

Contents lists available at ScienceDirect

Neurobiology of Disease

journal homepage: www.elsevier.com/locate/ynbdi

Istradefylline reduces memory deficits in aging mice with amyloid pathology

Anna G. Orr[a,b,*], Iris Lo[a], Heike Schumacher[a], Kaitlyn Ho[a], Michael Gill[a], Weikun Guo[a], Daniel H. Kim[a], Anthony Knox[a], Takashi Saito[c], Takaomi C. Saido[c], Jeffrey Simms[a], Carlee Toddes[a], Xin Wang[a], Gui-Qiu Yu[a], Lennart Mucke[a,b,**]

[a] Gladstone Institute of Neurological Disease, San Francisco, CA 94158, USA
[b] Department of Neurology, University of California, San Francisco, CA 94158, USA
[c] Laboratory for Proteolytic Neuroscience, RIKEN Brain Science Institute, Wako, Saitama 351-0198, Japan

ARTICLE INFO

Keywords:
Adenosine receptors
Alzheimer's disease
Amyloid plaques
Antagonist
Astrocytes
Behavior
Inhibition
Istradefylline
Memory
Therapy

ABSTRACT

Adenosine A_{2A} receptors are putative therapeutic targets for neurological disorders. The adenosine A_{2A} receptor antagonist istradefylline is approved in Japan for Parkinson's disease and is being tested in clinical trials for this condition elsewhere. A_{2A} receptors on neurons and astrocytes may contribute to Alzheimer's disease (AD) by impairing memory. However, it is not known whether istradefylline enhances cognitive function in aging animals with AD-like amyloid plaque pathology. Here, we show that elevated levels of Aβ, C-terminal fragments of the amyloid precursor protein (APP), or amyloid plaques, but not overexpression of APP per se, increase astrocytic A_{2A} receptor levels in the hippocampus and neocortex of aging mice. Moreover, in amyloid plaque-bearing mice, low-dose istradefylline treatment enhanced spatial memory and habituation, supporting the conclusion that, within a well-defined dose range, A_{2A} receptor blockers might help counteract memory problems in patients with Alzheimer's disease.

1. Introduction

Adenosine receptors regulate brain function and may have key roles in neurodegenerative disorders. Adenosine A_{2A} receptors (A_{2A}Rs) are highly expressed in inhibitory medium spiny neurons of the striatum and regulate the balance between the direct and indirect neural pathways controlling movement (Schwarzschild et al., 2006). A_{2A}R blockers enhance motor function in animal models of Parkinson's disease (PD). Istradefylline, a selective A_{2A}R blocker, is safe and well-tolerated (Kondo et al., 2015) and approved in Japan for the treatment of PD (Pinna, 2014).

In animal models, A_{2A}R blockade or removal ameliorated cognitive dysfunction resulting from acute brain trauma or seizures (Cognato et al., 2010; Ning et al., 2013). A_{2A}Rs expressed by neurons or astrocytes also contribute to cognitive deficits in models of Alzheimer's disease (AD) (Cunha et al., 2008; Laurent et al., 2016; Orr et al., 2015; Dall'Igna et al., 2007; Canas et al., 2009; Espinosa et al., 2013; Viana da Silva et al., 2016). Furthermore, we previously found that A_{2A}R levels on astrocytes were markedly increased in AD patients, and the increases correlated with disease severity (Orr et al., 2015). Gene-expression profiling in postmortem human brains revealed that A_{2A} mRNA levels correlate positively with frontal cortex atrophy in late-onset AD (Zhang et al., 2013). Moreover, genetic ablation of A_{2A}Rs in astrocytes enhanced reference memory in mice with or without AD-like plaque pathology (Orr et al., 2015), but impaired working memory in mice without plaques (Matos et al., 2015), supporting the notion that astrocytes regulate cognitive functions (Ransom and Ransom, 2012). These findings also suggest that alterations in A_{2A}R levels contribute to cognitive deficits in AD. However, it is uncertain what causes the increases in astrocytic A_{2A}R levels in AD and whether A_{2A}R antagonists can reduce cognitive deficits in the context of AD-like plaque pathology. Here, we analyzed A_{2A}R expression in APP transgenic mice with or without plaque pathology and assessed the effects of istradefylline on the behavior of plaque-bearing mice.

2. Materials and methods

2.1. Animals

Mice were housed in the Gladstone animal facility and treated in

* Correspondence to: A. Orr, Feil Family Brain and Mind Research Institute, Weill Cornell Medicine, 413 East 69th Street, New York, NY 10021, USA.
** Correspondence to: L. Mucke, Gladstone Institute of Neurological Disease, 1650 Owens Street, San Francisco, CA 94158, USA.
E-mail addresses: ago2002@med.cornell.edu (A.G. Orr), lennart.mucke@gladstone.ucsf.edu (L. Mucke).

https://doi.org/10.1016/j.nbd.2017.10.014
Received 18 July 2017; Received in revised form 26 September 2017; Accepted 27 October 2017
Available online 31 October 2017
0969-9961/

accordance with guidelines of the Institutional Animal Care and Use Committee, University of California, San Francisco. Mice were housed in groups of 2–5 per cage and maintained on a 12-h light/dark cycle with ad libitum access to food (PicoLab Rodent Diet 20, LabDiet, 5053) and water. All experiments were conducted during the light cycle and included littermate controls. Littermates were randomly assigned to a drug treatment condition, and groups of mice were balanced for age and sex as much as possible within each available cohort. Mice were treated, monitored and tested by experimenters blinded to the genotypes and treatment conditions. Human amyloid precursor protein (hAPP) transgenic mice from line J20 (hAPP-J20 mice, C57BL/6) express an alternatively spliced human *APP* minigene encoding hAPP695, hAPP751 and hAPP770 with the Swedish and Indiana familial AD mutations directed by the *PDGF* β-chain promoter (Mucke et al., 2000; Palop et al., 2007). hAPP-I5 mice (C57BL/6, line I5) express a human *APP* minigene directed by the *PDGF* β-chain promoter that encodes wildtype hAPP695, hAPP751 and hAPP770 without familial AD mutations (Mucke et al., 2000). Homozygous *APP* knock-in ($APP^{NL\text{-}G\text{-}F}$) mice have two mouse *App* alleles bearing the Swedish, Beyreuther/Iberian and Arctic familial AD mutations as well as a humanized Aβ sequence (Saito et al., 2014). This study was approved by the Institutional Animal Care and Use Committee, and all experiments were conducted in accordance with the United States Public Health Service's Policy on Humane Care and Use of Laboratory Animals.

2.2. Drug preparation and administration

Istradefylline was obtained in powder form (Tocris, 5147) and is highly insoluble in water. To enable daily oral intake of istradefylline in the drinking water, we tested a variety of solubilizing agents. We found that istradefylline was not fully solubilized and gradually precipitated in solutions with < 30% DMSO or in 0.25–1% methylcellulose. Although a mixture of 40% DMSO and 60% Cremophor EL (Sigma) effectively solubilized the drug, daily fluid intake of the final treatment solution was reduced in mice, possibly due to the odor of Cremophor EL. We therefore reduced the amount of Cremophor EL by substitution with mineral oil. The final formulation for solubilizing the drug consisted of 40% DMSO, 30% Cremophor EL and 30% mineral oil. The solubilized drug stock was further diluted in 2% sucrose in water to prepare the final treatment solutions, which contained 0.2–2% DMSO, 0.15–1.5% Cremophor EL, and 0.15–1.5% mineral oil, depending on the specific drug dose. We used low concentrations of DMSO and the amounts that reached the brain after ingestion were likely much lower (Kaye et al., 1983). However, because DMSO can affect various biological processes, including AD-linked cascades (Julien et al., 2012), the vehicle solutions contained the same final concentrations of solubilizing agents and sucrose as the drug solutions, but did not contain istradefylline.

All final solutions were prepared daily and were protected from light with aluminum foil. Mice received drug or vehicle solutions in 50-ml tubes with attached spouts placed in their home cages and did not have access to other sources of fluids during treatment, which continued for the duration of behavioral testing. Body weight, chow intake and daily fluid intake were closely monitored (Suppl. Figs. 1–2). To habituate the mice to the bottles and the vehicle solutions, the mice were first given bottles with plain water for 2–3 days followed by vehicle solution for another 2–3 days. Subsequently, half of the mice were given bottles with vehicle solution containing istradefylline. The route of administration and dosing were chosen based on the drug's pharmacokinetic properties (Yang et al., 2007) and previous studies (Cognato et al., 2010). To achieve the desired drug dose in male and female mice, average body weight and daily fluid intake were used to calculate the required drug concentrations in the solutions.

For cohorts receiving 4 or 40 mg/kg/day, open-field experiments were started 1–3 days after drug treatment was initiated. For cohorts receiving 10 or 15 mg/kg/day, open-field experiments were started two weeks after drug treatment was initiated. The longer time-points were designed to eliminate the potential confound of behavioral testing before steady-state drug levels were reached. All Morris water maze (MWM) experiments were performed three weeks after drug treatment was initiated. Mice were tested in the elevated plus maze and the Rotarod two and five weeks after treatment was initiated, respectively.

To measure istradefylline levels in the plasma and brain, mice were treated with drug or vehicle as indicated, anesthetized with Avertin (tribromoethanol, 250 mg/kg) and perfused transcardially with 0.9% saline for 1 min. Cardiac blood was collected in anesthetized mice immediately before perfusion. The plasma was isolated by centrifugation at 3000 rpm for 15 min at 4 °C. Istradefylline concentrations in the plasma and snap-frozen hemibrains were measured by Brains Online using HPLC with tandem mass spectrometry and internal standards. Notably, istradefylline isomerizes when exposed to light (Hockemeyer et al., 2004). Indeed, the chromatograms showed two peaks for istradefylline. Calculations for each peak were made assuming that the racemic mixture consisted of equal parts of each isomer. E isomers may have higher adenosine receptor affinity than Z isomers (Muller et al., 1997). The reported concentrations are the sum of the two isomers. Non-terminal blood collection was performed by submandibular bleeding in mice under brief isoflurane anesthesia.

We performed a pilot dosing study in 9–16-month-old wild-type (WT) male and female C57Bl/6 mice, which showed that oral intake of istradefylline resulted in dose-dependent increases in plasma levels of the drug by days 3 and 8 (Suppl. Fig. 3A). Approximately 75% of fluid intake in C57Bl/6 mice occurs during the dark phase (Gordon et al., 1986), which might be expected to cause reductions in the levels of drug during the light phase. However, we did not observe reductions in plasma drug levels in the late afternoon (approximately 4 PM) as compared to the morning (approximately 9 AM) (Suppl. Fig. 3A), suggesting that drug levels were relatively stable throughout the day. Istradefylline treatment at 40 mg/kg/day for 25 days resulted in comparable plasma drug levels in 18–19-month-old WT and hAPP-J20 mice (Suppl. Fig. 3B). Following a 10-day washout period, the levels of drug in the plasma were markedly reduced (Suppl. Fig. 3B). Chronic treatment with 4–15 mg/kg/day resulted in dose-dependent increases in the levels of drug in brain tissue in WT and hAPP-J20 mice (Suppl. Fig. 3C).

2.3. Behavioral testing

For all behavioral testing, the experimenters were blinded to the genotype and treatment of the mice. Mice that showed poor health or injuries that interfered with behavioral testing (for example, skin lesions, eye injury, tumors, slowed movement or inability to swim) were excluded from the analyses. The incidence of such health problems was not different between drug-treated and placebo-treated mice (data not shown). Behavioral data were obtained with the help of the Gladstone Institutes' Behavioral Core.

2.4. Morris water maze

The maze consisted of a 122-cm-diameter pool filled with water (20 ± 2 °C) made opaque with nontoxic white tempera paint. The pool was surrounded with distinct extra-maze cues. Before hidden platform training, all mice underwent one session of 3–4 pre-training trials in which they swam in a rectangular channel (15 cm × 122 cm) and mounted a square platform (14 × 14 cm) hidden 1 cm below the water surface in the middle of the channel. If a mouse did not mount the platform within 10 s, it was guided to the platform by the experimenter and was allowed to sit on the platform for 10 s before it was removed by the experimenter. The day after pre-training, mice were trained in the circular water maze. For hidden platform training, the platform was submerged 1.5 cm below the surface. The platform location remained the same throughout training, but the drop location varied randomly among the four daily trials. Mice received two sessions per day (3-h

interval between sessions) for 8 consecutive days. Each session consisted of two trials with a 15-min interval. The maximum time allowed per trial was 60 s. If a mouse did not find or mount the platform, it was guided to the platform by the experimenter. All mice were allowed to sit on the platform for 15 s after each training trial.

For probe trials, the platform was removed and each mouse was allowed to swim for 60 s. The drop location for the probe trials was 180° from the platform location used during hidden platform training. After 60 s, mice were guided to the platform location before removal from the pool. Mice were probed on days 1 and 3 after hidden platform training. After probe testing, cued (visible) platform training was performed using a new platform location and a clearly visible cue (a 15-cm pole on top of the platform). Mice received three sessions of two cued trials per session in one day (10-min interval between trials and 2-h interval between sessions). All behavior was recorded and analyzed with an Ethovision XT video tracking system (Noldus). Escape latencies, distance traveled, swim paths, swim speeds, platform crossings and proximity to the platform were recorded automatically for subsequent analysis.

2.5. Open-field test

Spontaneous movement, rearing and context-dependent habituation in the open field were measured with an automated Flex-Field/Open Field Photobeam Activity System (San Diego Instruments, San Diego, CA). After acclimation to the testing room for 1 h, mice were placed individually in a clear plastic chamber (41 × 41 × 30 cm) with two 16 × 16 photobeam arrays detecting horizontal and vertical movements. Chambers were surrounded by distinct proximal cues. Mice were exposed to the chambers in 5-min trials (2 trials per day with a 3-h inter-trial interval) and tested in the same chambers 3–5 weeks later. The apparatus was cleaned with 70% alcohol after each mouse. Total movements (ambulations), rearings, and time spent in the center versus periphery of the open field were recorded automatically by the system for subsequent analysis.

2.6. Elevated plus maze

The maze consisted of two open and two enclosed arms elevated 63 cm above the ground (Hamilton-Kinder, Poway, CA). After acclimation to the testing room for 1 h, mice were placed at the junction between the open and closed arms of the maze and allowed to explore freely for 5 min. The maze was cleaned with 70% ethanol after each mouse. Total distance traveled and time spent in the open and closed arms were recorded automatically for subsequent analysis.

2.7. Rotarod test

After acclimation to the testing room for 1 h, mice were placed on the Rotarod (Med Associates Inc.), which was rotated at a constant speed of 16 rpm on day 1 and at increasing speeds (4–40 rpm) on day 2. Photobeam interruptions caused by mice falling off the rotating rod were recorded. Photobeams were interrupted by the experimenter if the mouse held onto the rod without walking for three full rotations. Each mouse was given three trials with a 10-min inter-trial interval and a maximum of 300 s per trial. The average latency to fall off the Rotarod was calculated.

2.8. Immunohistochemistry

Mice were anesthetized with Avertin (tribromoethanol, 250 mg per kg) and perfused with 0.9% saline for 1 min. Brains were removed, post-fixed in 4% paraformaldehyde, incubated in 30% sucrose for 1–3 days at 4 °C, and sectioned at a thickness of 30 μm using a freezing microtome (Leica SM 2000R). Sections were incubated for 15 min in 0.3% Sudan black (Sigma-Aldrich) with 70% ethanol to block autofluorescence and for 2 h in blocking reagent provided in the mouse-on-mouse kit (Vector Laboratories). Sections were then incubated overnight at room temperature in mouse anti-A_{2A} receptor IgG2a antibody (1:200, Millipore, 05-717), mouse anti-GFAP IgG1 antibody (1:1000, Millipore, MAB360), and rabbit anti-human amyloid-β (N) IgG antibody (1:250, IBL-America, 18584), followed by a 1-h incubation at room temperature with goat anti-mouse IgG2a-488, goat anti-mouse IgG1-546 and goat anti-rabbit IgG-648. Sections were mounted onto slides with Prolong Diamond anti-fade reagent (Thermo Fisher Scientific). Selectivity of the A_{2A} receptor antibody was confirmed using brain sections from A_{2A} knockout mice, as reported previously (Orr et al., 2015).

Brain sections were imaged using a 10 × objective (Keyence) and analyzed with a BZ-9000 automated microscope system and analysis application (Keyence). A_{2A} and GFAP immunoreactivities were quantified in the stratum radiatum of the CA1 region of the dorsal hippocampal formation and in the somatosensory cortex using two sections per mouse. A_{2A} receptor and GFAP immunoreactivities were also observed in the dorsal hippocampus (data not shown). To obtain high-resolution photomicrographs, multiple images were acquired and reconstructed automatically for each brain section. After cropping the images to isolate the CA1 and somatosensory cortex, thresholding was carried out using a constant intensity value to separate background staining from the signal of interest. Regions of interest were automatically visualized and quantified to obtain the total area of the cropped region and the total area of immunoreactivity per section. These values were averaged per mouse and compared between genotypes.

2.9. Statistics

Unless indicated otherwise, data are presented as means ± SEM. All statistical tests except for the data shown in Fig. 2A were performed with GraphPad Prism (version 5). In Fig. 2A, the learning curves were analyzed using rank-summary scoring and linear regression (Possin et al., 2016) in R software (R Development Core Team, 2015). Sample sizes were determined based on pilot experiments and previous studies including similar types of experiments. Normality was tested by D'Agostino and Pearson omnibus normality test. The criterion for data point exclusion was established during the design of the study and was set to values above or below two standard deviations from the group mean. We excluded 7 mice (5 WT and 2 hAPP-J20 mice) from behavioral testing due to sporadic health issues, such as eye damage and skin lesions. Variances were compared by F test or Bartlett's test. Differences between two groups were assessed by unpaired two-tailed Student's *t*-test and FDR correction for multiple comparisons. Welch's correction was used to account for unequal variances between two groups. Differences among treatment groups were assessed by one-way or two-way ANOVA followed by Dunnett's or Bonferroni post-test, respectively.

3. Results

Similar to AD patients, hAPP-J20 mice form amyloid plaques and show progressive increases in astrocytic A_{2A}R levels (Orr et al., 2015). These mice overexpress familial AD-mutant forms of hAPP in neurons and have pathologically elevated cerebral levels of amyloid-β (Aβ), the main constituent of amyloid plaques, and other AD-like abnormalities (Palop and Mucke, 2016; Musiek and Holtzman, 2015). The close temporal and spatial association between amyloid deposition and astrocytic A_{2A}R expression suggests that the latter may be caused by amyloid plaques, similar to other plaque-associated changes observed in AD (Serrano-Pozo et al., 2016). Alternatively, the increase in astrocytic A_{2A}Rs may be caused by overexpression of hAPP together with biological aging or the passage of time. To test this alternate hypothesis, we studied hAPP mice from line I5, which overexpress wildtype hAPP

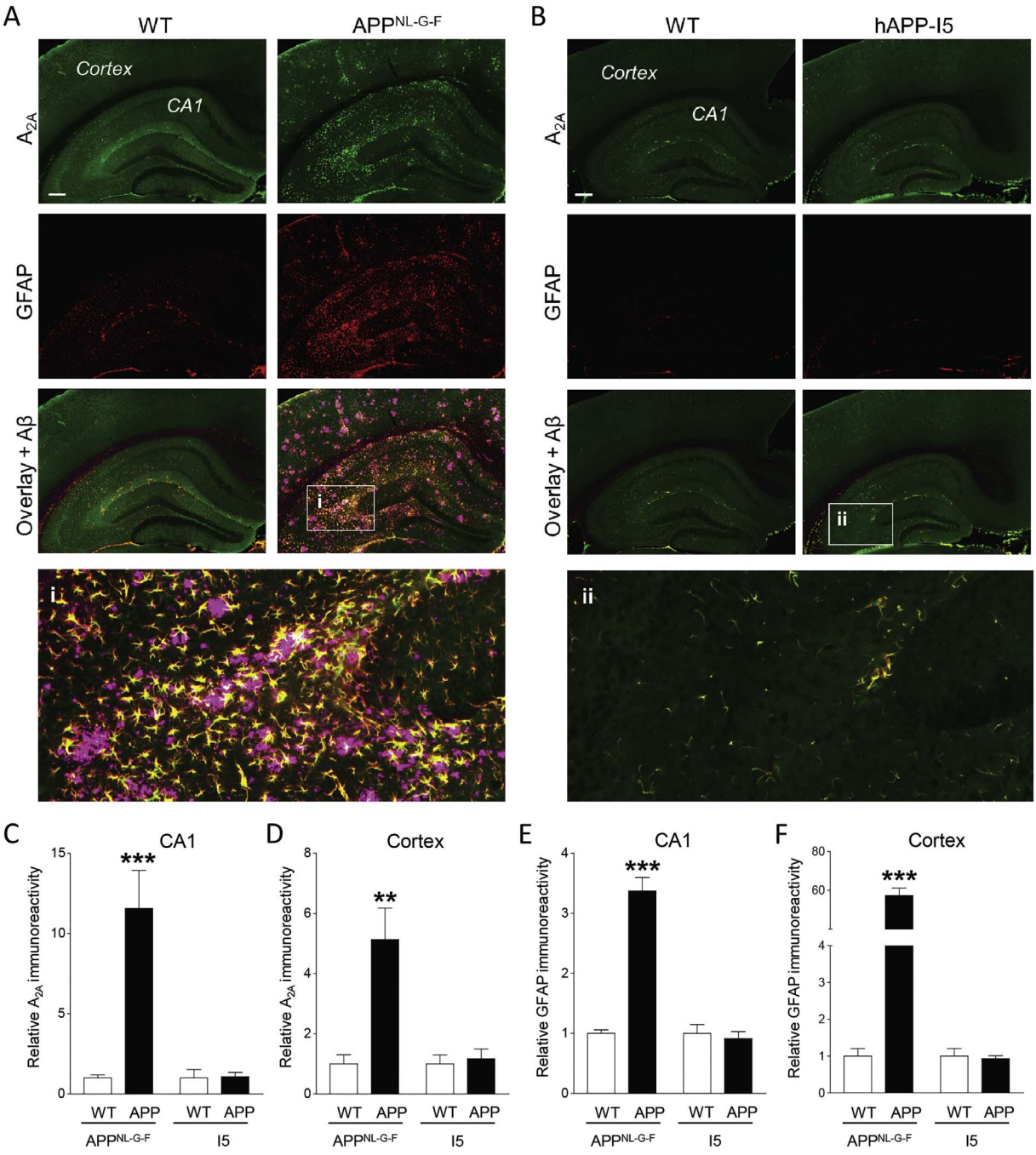

Fig. 1. Increases in A_{2A} levels in mice with amyloid-β accumulation.
(A and B) Representative photomicrographs of hippocampal and neocortical sections from 9–10-month-old $APP^{NL\text{-}G\text{-}F}$ (A) and hAPP-I5 (B) mice and age-matched wildtype (WT) controls (A and B) immunostained for the $A_{2A}R$ (green), GFAP (red) and Aβ (magenta). Overlay of $A_{2A}R$ and GFAP is shown in yellow. Insets (i–ii) show magnified views of the boxed regions. Scale bars: 200 μm. (C–F) Levels of $A_{2A}R$ and GFAP immunoreactivities in CA1 and neocortex normalized to total selected brain areas and averages in WT littermates. $A_{2A}R$: $n = 4$ WT mice (from $APP^{NL\text{-}G\text{-}F}$ line), 14 $APP^{NL\text{-}G\text{-}F}$ mice, 6 WT mice (from hAPP-I5 line), 15 hAPP-I5 mice. GFAP: $n = 4$ WT mice (from $APP^{NL\text{-}G\text{-}F}$ line), 9 $APP^{NL\text{-}G\text{-}F}$ mice, 6 WT mice (from hAPP-I5 line), 10 hAPP-I5 mice. $^{**}P < 0.01$, $^{***}P < 0.001$ vs. WT littermate controls (*t*-test with Welch's correction). Values are means ± SEM.

and never form amyloid plaques (Mucke et al., 2000), and *App* knock-in ($APP^{NL\text{-}G\text{-}F}$) mice, which do not overexpress hAPP or mouse APP but—like hAPP-J20 mice—overproduce amyloidogenic human Aβ and the C-terminal APP fragment C99, form amyloid plaques, and develop astrocytosis and memory loss (Saito et al., 2014; Masuda et al., 2016) (and data not shown).

Like hAPP-J20 and hAPP/PS1 mice (Orr et al., 2015), plaque-bearing $APP^{NL\text{-}G\text{-}F}$ mice had increased levels of glial fibrillary acidic protein (GFAP), indicating reactive astrocytosis, and increased astrocytic $A_{2A}R$ levels in the hippocampus and neocortex, whereas such increases were not found in hAPP-I5 mice (Fig. 1). Thus, hAPP overexpression per se did not cause the astrocytic alterations. Since hAPP-J20 and $APP^{NL\text{-}G\text{-}F}$ mice have normal astrocytic $A_{2A}R$ levels before they form amyloid plaques (Orr et al., 2015) (and data not shown), accumulation of amyloid plaques is the likeliest cause of increased astrocytic $A_{2A}R$ expression in these models and, possibly, also in the human condition. We cannot rule out contributions from pathologically elevated levels of soluble Aβ assemblies (particularly oligomers). Indeed, application of $Aβ_{1–42}$ increased the levels of $A_{2A}R$ in primary astrocyte cultures (Matos et al., 2012). Increased C99 levels, which occur in

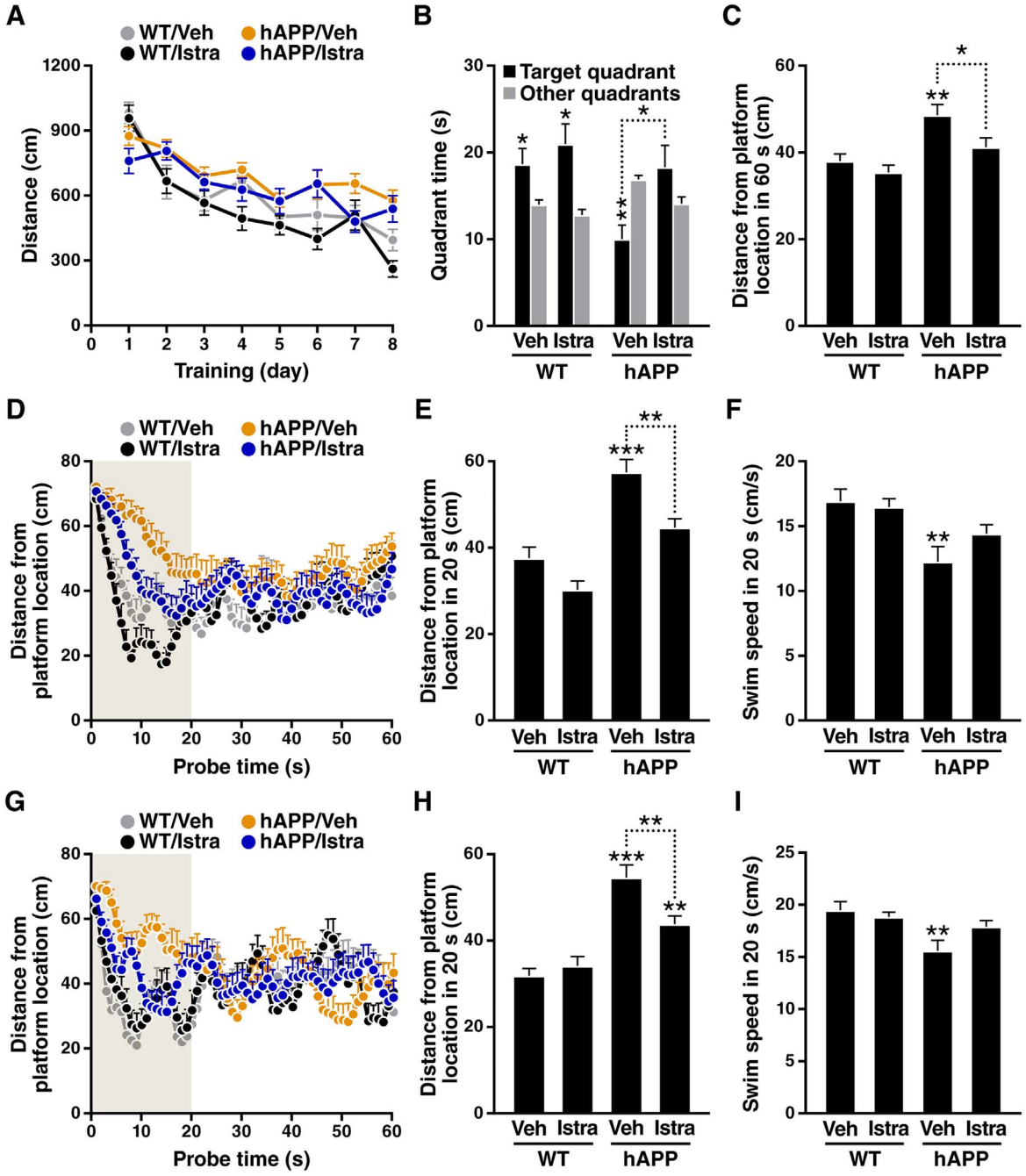

Fig. 2. Istradefylline enhances spatial memory in hAPP mice.

14–15-month-old WT and hAPP-J20 mice treated with vehicle (Veh) or istradefylline (Istra, 10 mg/kg/day) were tested in the Morris water maze. (A) Distance traveled during hidden platform training (four trials/day). Linear regression analysis: t = 2.966, $P = 0.0045$ for genotype effect; t = −1.583, $P = 0.112$ for drug effect; t = −0.019, $P = 0.99$ for interaction effect. n = 14–16 mice per genotype and treatment. (B–I) Probe trials 1 day (B–F) and 3 days (G–I) after training. (B) Time in target and nontarget (other) quadrants. Two-way ANOVA of target quadrant time: $F(1,52) = 5.66$, $P = 0.0211$ for drug effect; $F(1,52) = 6.42$, $P = 0.0143$ for genotype effect. t-test with FDR correction for multiple comparisons (target vs. other quadrants): $P = 0.044$ (WT/Veh), 0.012 (WT/Istra), 0.008 (hAPP/Veh), 0.14 (hAPP/Istra). n = 13–15 mice per genotype and treatment. (C–E) Distance from the platform location. Average distance in 60 s (C–D) and the first 20 s (E) of the 24-hour probe trial. Two-way ANOVA: (C) $F(1,53) = 4.93$, $P = 0.0307$ for drug effect; $F(1,53) = 13.37$, $P = 0.0006$ for genotype effect. n = 13–16 mice per genotype and treatment. (E) $F(1,51) = 14.46$, $P = 0.0004$ for drug effect; $F(1,51) = 42.22$, $P < 0.0001$ for genotype effect. n = 3–15 mice per genotype and treatment. (F) Swim speed. Two-way ANOVA: $F(1,52) = 12.40$, $P = 0.0009$ for genotype effect. n = 14–16 mice per genotype and treatment. (G and H) Distance from the platform location. Average distance in 60 s (G) and the first 20 s (H) of the 72-hour probe trial. Two-way ANOVA: (H) $F(1,52) = 7.20$, $P = 0.0098$ for interaction effect; $F(1,52) = 44.54$, $P < 0.0001$ for genotype effect. n = 13–16 mice per genotype and treatment. (I) Swim speed. Two-way ANOVA: $F(1,53) = 8.30$, $P = 0.0057$ for genotype effect. n = 13–16 mice per genotype and treatment. $^*P < 0.05$, $^{**}P < 0.01$, $^{***}P < 0.001$ vs. other quadrants by t-test (B) or WT/Veh group by Dunnett's test (C, E, F, H, I), or as indicated by the brackets (Bonferroni test). Shading indicates the first 20 s of the probe trial. Values are means ± SEM.

hAPP-J20 and $APP^{NL\text{-}G\text{-}F}$ mice and in humans with some familial forms of AD (Sahlin et al., 2007), may have contributed also. Furthermore, APP metabolites are not the only factors that can increase astrocytic $A_{2A}R$ expression (Orr et al., 2015).

In 14–21-month-old WT mice and hAPP-J20 mice, administration of istradefylline in the drinking water caused dose-dependent increases of drug levels in plasma and brain (Suppl. Fig. 3). In pilot experiments, doses higher than 10 mg/kg/day increased total movements and rearing in both genotypes (Suppl. Fig. 4), consistent with reports that istradefylline enhances locomotion (Yu et al., 2008; Bastia et al., 2005).

To avoid this potential confound, mice were treated with 4 or 10 mg/kg/day.

The effects of istradefylline on learning and memory were tested with the Morris water maze. To escape the water, mice must learn to use extramaze visual cues to locate a hidden platform (Morris, 1984). After training, the platform is removed and probe trials are done to assess spatial memory. Three weeks of drug treatment at either dose did not affect learning in training trials (Fig. 2A; Suppl. Fig. 5A). In probe trials 1 day after training, hAPP-J20 mice treated with 10 mg/kg/day spent more time in the target quadrant (Fig. 2B) than vehicle-treated hAPP-J20 mice and achieved better average proximity to the platform location (Fig. 2C), a sensitive measure of spatial memory (Possin et al., 2016; Maei et al., 2009; Gallagher et al., 1993).

As shown by proximity to platform location, vehicle-treated hAPP-J20 mice had the most prominent deficits during the first 20 s of the probe trial relative to vehicle-treated WT mice (Fig. 2D and G; Suppl. Figs. 5B and 6A–C), possibly because their search strategy improved with time. Since the platform was no longer at the expected location, learning-dependent extinction or changes in the search strategy of WT mice may have contributed also (Maei et al., 2009). hAPP-J20 mice treated with 4 or 10 mg/kg/day performed better than vehicle-treated hAPP-J20 mice during the first 20 s of the probe trial (Fig. 2E; Suppl. Fig. 5C). In a second probe trial 3 days after training, hAPP-J20 mice treated with 10 mg/kg/day again showed enhanced performance (Fig. 2G, H). Drug-treated hAPP-J20 mice also had faster swim speeds than vehicle-treated hAPP-J20 mice (Fig. 2F and I). However, drug treatment did not affect swim speeds during training (Suppl. Fig. 7A) or enhance motor performance in the Rotarod test (Suppl. Fig. 7B, C), suggesting that the treatment did not increase locomotor function per se.

At 15 mg/kg/day, istradefylline did not affect learning (Suppl. Fig. 6A) but impaired probe performance of WT mice and did not improve the performance in hAPP-J20 mice (Suppl. Fig. 6B–F). Thus, in aging mice with chronic plaque pathology, istradefylline enhances spatial memory primarily at low doses.

Istradefylline at doses of 4, 10 and 15 mg/kg/day also improved learning of the cued navigation task in hAPP-J20 mice (Suppl. Fig. 8), possibly due to improvements in striatum-dependent navigation to the visible platform (Rice et al., 2015). In contrast, istradefylline treatment did not affect performance during hidden platform training (Fig. 2A; Suppl. Figs. 5A and 6A), which involves distal cues and is dependent on hippocampal function.

We also examined the effects of istradefylline in the open-field test, in which mice were habituated to an arena by repeated exposures. At 4 mg/kg/day, istradefylline enhanced context habituation in WT and hAPP-J20 mice (Suppl. Fig. 9A, B), which provides another putative measure of learning and memory (Vianna et al., 2000). Three weeks after habituation, drug-treated WT and hAPP-J20 mice still showed fewer movements in the familiar context (Suppl. Fig. 9C). At 10 mg/kg/day, istradefylline had similar effects (Suppl. Fig. 9E, F). Decreased locomotion has been reported for chronic intake of caffeine (Nikodijevic et al., 1993), a nonselective adenosine receptor blocker, and genetic deletion of the $A_{2A}R$ (Kachroo et al., 2005; Wang et al., 2006), but—to our knowledge—not yet for istradefylline or other selective $A_{2A}R$ antagonists.

Istradefylline did not affect time spent in the center of the open field (Suppl. Fig. 9D) and increased the amount of time spent in the open arms of the elevated plus maze (Suppl. Fig. 10), suggesting that istradefylline did not increase anxiety-like behaviors. Thus, besides enhancing spatial memory and cued navigation in aging hAPP-J20 mice, $A_{2A}R$ blockade improved context habituation without reducing motor ability or increasing anxiety.

4. Discussion

Our findings suggest that amyloid deposition is a strong causal driver of the striking increase in astrocytic $A_{2A}R$ expression we previously discovered in AD patients and related animal models (Orr et al., 2015). We also demonstrate that istradefylline treatment can improve memory in the context of AD-related plaque pathology in aging mice. Notably, this beneficial effect was observed at relatively low doses, whereas a higher dose had no effect on probe performance in plaque-bearing mice. Interestingly, other memory-enhancing agents such as cholinergic and noradrenergic agonists also had U- or J-shaped dose-response curves in different species and behavioral paradigms (Baldi and Bucherelli, 2005). Caffeine, a nonselective blocker of $A_{2A}R$, had various beneficial effects in animal models of amyloid pathology and enhanced memory consolidation in humans (Arendash et al., 2006; Cao et al., 2012; Borota et al., 2014). In light of these findings, the use of istradefylline in the treatment of PD patients and ongoing trials with other $A_{2A}R$ blockers, it would be interesting to determine whether these drugs could also improve cognitive functions in patients with AD.

Like other neurotherapeutics, istradefylline appears to have a narrow therapeutic window, showing beneficial effects in aging mice only at doses ≤ 10 mg/kg/day in our study. In a nonhuman primate model of PD, istradefylline also reduced cognitive deficits only at the lowest dose (Ko et al., 2016). Age and other variables can shift therapeutic windows (Calabrese, 2008). Similar shifts during AD might require patient stratification and dose adjustments based on biomarkers and end points that correlate with drug efficacy (Jack and Holtzman, 2013). Molecular imaging of aberrant increases in $A_{2A}R$ levels and drug occupancy in extrastriatal regions of the brain, particularly the hippocampus, with radiopharmaceutical ligands and PET scanning (Rissanen et al., 2013; Tavares et al., 2013) might be used to select patients and guide adaptive dosing. These strategies could also help identify the stage(s) when $A_{2A}R$ blockers might be most effective in AD. Our results in transgenic mice and AD patients suggest that $A_{2A}R$ receptor levels in astrocytes closely relate to plaque pathology and disease stage (this study and ref. (Orr et al., 2015)), although a variety of additional factors might affect when and how astrocytes, neurons and other cell types express these receptors in AD.

As discussed previously (Chen et al., 2007; Cunha, 2005), low doses of $A_{2A}R$ antagonists may cause a different set of behavioral effects than high doses by engaging different neural systems or the same neural systems in a different manner. Indeed, low-dose (4 or 10 mg/kg/day) istradefylline treatment enhanced habituation and spatial memory without increasing movements in aging hAPP-J20 mice, whereas the 15 mg/kg/day dose elicited modest alterations in locomotion and the 40 mg/kg/day dose triggered robust hyperlocomotion. These results are consistent with previous studies demonstrating different dose-dependent effects of $A_{2A}R$ antagonists in animal models of striatal damage (Popoli et al., 2002; Blum et al., 2003).

In healthy brains, $A_{2A}Rs$ are most highly expressed by striatal inhibitory neurons and moderately expressed by other neurons (Burnstock, 2007). The striatum is critical for movement control, and genetic ablation of $A_{2A}Rs$ in inhibitory neurons prevents istradefylline-induced hyperactivity (Shen et al., 2008). Intriguingly, ablation of $A_{2A}Rs$ in inhibitory neurons worsened probe performance in the water maze without affecting learning (Wei et al., 2011). Thus, blockade of $A_{2A}Rs$ on inhibitory neurons might counteract the memory-enhancing effects of istradefylline and mediate the worsening of probe performance at higher doses.

$A_{2A}Rs$ may regulate locomotion and affect neuronal health by distinct mechanisms (Yu et al., 2008; Chen et al., 2007), including through effects on presynaptic and postsynaptic neuronal activities and on glial functions (Orr et al., 2015; Yu et al., 2008; Shen et al., 2013; Orr et al., 2009; Rebola et al., 2011; Gyoneva et al., 2014; Madeira et al., 2016). In addition, short-term pharmacological blockade is likely to induce a distinct set of biological effects than chronic genetic ablation of the receptor, due to differences in how receptor function is affected and what compensatory and feedback mechanisms are activated in each scenario.

The presence and extent of neuropathological alterations may have a strong impact on the overall effect of modulating A_{2A}Rs. In young hAPP mice without prominent plaque deposition or astrogliosis, knockdown of A_{2A}Rs in CA3 neurons reduced deficits in synaptic plasticity (Viana da Silva et al., 2016). Ablation of A_{2A}Rs in excitatory forebrain neurons did not enhance reference memory in mice without hAPP expression (Wei et al., 2011; Kaster et al., 2015), but reduced learning and memory deficits in a model of chronic stress (Kaster et al., 2015). In addition, optogenetic activation of chimeric A_{2A}Rs in excitatory neurons impaired working memory (Li et al., 2015). Like humans with AD, aging hAPP mice have prominent plaque pathology and marked increases in A_{2A}R expression. In this AD-relevant context, both genetic ablation of A_{2A}Rs in astrocytes (Orr et al., 2015) and low-dose istradefylline treatment (this study) reduced memory problems. Thus, the specific effects of A_{2A}R ablation or blockade are likely determined by the most prominently affected cell populations and by neuropathological processes that alter A_{2A}R distribution and activity in different cell types. Additional studies are needed to unravel the mechanisms of these differential effects and to explore the therapeutic potential of A_{2A}R antagonists in AD and related conditions.

Conflict of interest

None.

Acknowledgements

We thank Pascal Sanchez for helpful discussions; Isabel Lopez, Sharon Lee, and Xinxing Yu for technical support; Stephen Ordway for editorial review; and Courtney Dickerson and Joy Lingat for administrative assistance. This study was supported by NIH grants K99AG048222 (AGO) and P30NS065780 (LM), P50AG023501, Alan Kaganov Scholarship (AGO), S.D. Bechtel, Jr. Foundation (LM), MetLife Foundation (LM), and Dolby Family (LM). The Gladstone Institutes received support from National Center for Research Resources Grant RR18928.

Appendix A. Supplementary data

Supplementary data to this article can be found online at https://doi.org/10.1016/j.nbd.2017.10.014.

References

Arendash, G.W., Schleif, W., Rezai-Zadeh, K., et al., 2006. Caffeine protects Alzheimer's mice against cognitive impairment and reduces brain β-amyloid production. Neuroscience 142, 941–952.
Baldi, E., Bucherelli, C., 2005. The inverted "u-shaped" dose-effect relationships in learning and memory: modulation of arousal and consolidation. Nonlinearity Biol. Toxicol. Med. 3, 9–21.
Bastia, E., Xu, Y.H., Scibelli, A.C., et al., 2005. A crucial role for forebrain adenosine A_{2A} receptors in amphetamine sensitization. Neuropsychopharmacology 30, 891–900.
Blum, D., Galas, M.C., Pintor, A., et al., 2003. A dual role of adenosine A_{2A} receptors in 3-nitropropionic acid-induced striatal lesions: implications for the neuroprotective potential of A_{2A} antagonists. J. Neurosci. 23, 5361–5369.
Borota, D., Murray, E., Keceli, G., et al., 2014. Post-study caffeine administration enhances memory consolidation in humans. Nat. Neurosci. 17, 201–203.
Burnstock, G., 2007. Physiology and pathophysiology of purinergic neurotransmission. Physiol. Rev. 87, 659–797.
Calabrese, E.J., 2008. Alzheimer's disease drugs: an application of the hormetic dose-response model. Crit. Rev. Toxicol. 38, 419–451.
Canas, P.M., Porciuncula, L.O., Cunha, G.M., et al., 2009. Adenosine A_{2A} receptor blockade prevents synaptotoxicity and memory dysfunction caused by β-amyloid peptides via p38 mitogen-activated protein kinase pathway. J. Neurosci. 29, 14741–14751.
Cao, C., Loewenstein, D.A., Lin, X., et al., 2012. High blood caffeine levels in MCI linked to lack of progression to dementia. J. Alzheimers Dis. 30, 559–572.
Chen, J.F., Sonsalla, P.K., Pedata, F., et al., 2007. Adenosine A_{2A} receptors and brain injury: broad spectrum of neuroprotection, multifaceted actions and "fine tuning" modulation. Prog. Neurobiol. 83, 310–331.
Cognato, G.P., Agostinho, P.M., Hockemeyer, J., et al., 2010. Caffeine and an adenosine A_{2A} receptor antagonist prevent memory impairment and synaptotoxicity in adult rats triggered by a convulsive episode in early life. J. Neurochem. 112, 453–462.
Cunha, R.A., 2005. Neuroprotection by adenosine in the brain: from A_1 receptor activation to A_{2A} receptor blockade. Purinergic Signal 1, 111–134.
Cunha, G.M., Canas, P.M., Melo, C.S., et al., 2008. Adenosine A_{2A} receptor blockade prevents memory dysfunction caused by β-amyloid peptides but not by scopolamine or MK-801. Exp. Neurol. 210, 776–781.
Dall'Igna, O.P., Fett, P., Gomes, M.W., et al., 2007. Caffeine and adenosine A_{2a} receptor antagonists prevent β-amyloid (25–35)-induced cognitive deficits in mice. Exp. Neurol. 203, 241–245.
Espinosa, J., Rocha, A., Nunes, F., et al., 2013. Caffeine consumption prevents memory impairment, neuronal damage, and adenosine A_{2A} receptors upregulation in the hippocampus of a rat model of sporadic dementia. J. Alzheimers Dis. 34, 509–518.
Gallagher, M., Burwell, R., Burchinal, M., 1993. Severity of spatial learning impairment in aging: development of a learning index for performance in the Morris water maze. Behav. Neurosci. 107, 618–626.
Gordon, M.N., Osterburg, H.H., May, P.C., et al., 1986. Effective oral administration of 17 β-estradiol to female C57BL/6J mice through the drinking water. Biol. Reprod. 35, 1088–1095.
Gyoneva, S., Shapiro, L., Lazo, C., et al., 2014. Adenosine A_{2A} receptor antagonism reverses inflammation-induced impairment of microglial process extension in a model of Parkinson's disease. Neurobiol. Dis. 67, 191–202.
Hockemeyer, J., Burbiel, J.C., Muller, C.E., 2004. Multigram-scale syntheses, stability, and photoreactions of A_{2A} adenosine receptor antagonists with 8-styrylxanthine structure: potential drugs for Parkinson's disease. J. Organomet. Chem. 69, 3308–3318.
Jack Jr., C.R., Holtzman, D.M., 2013. Biomarker modeling of Alzheimer's disease. Neuron 80, 1347–1358.
Julien, C., Marcouiller, F., Bretteville, A., et al., 2012. Dimethyl sulfoxide induces both direct and indirect tau hyperphosphorylation. PLoS One 7, e40020.
Kachroo, A., Orlando, L.R., Grandy, D.K., et al., 2005. Interactions between metabotropic glutamate 5 and adenosine A_{2A} receptors in normal and parkinsonian mice. J. Neurosci. 25, 10414–10419.
Kaster, M.P., Machado, N.J., Silva, H.B., et al., 2015. Caffeine acts through neuronal adenosine A_{2A} receptors to prevent mood and memory dysfunction triggered by chronic stress. Proc. Natl. Acad. Sci. U. S. A. 112, 7833–7838.
Kaye, T.S., Egorin, M.J., Riggs Jr., C.E., et al., 1983. The plasma pharmacokinetics and tissue distribution of dimethyl sulfoxide in mice. Life Sci. 33, 1223–1230.
Ko, W.K., Camus, S.M., Li, Q., et al., 2016. An evaluation of istradefylline treatment on Parkinsonian motor and cognitive deficits in 1-methyl-4-phenyl-1,2,3,6-tetrahydropyridine (MPTP)-treated macaque models. Neuropharmacology 110, 48–58.
Kondo, T., Mizuno, Y., Japanese Istradefylline Study Group, 2015. A long-term study of istradefylline safety and efficacy in patients with Parkinson disease. Clin. Neuropharmacol. 38, 41–46.
Laurent, C., Burnouf, S., Ferry, B., et al., 2016. A_{2A} adenosine receptor deletion is protective in a mouse model of Tauopathy. Mol. Psychiatry 21, 149.
Li, P., Rial, D., Canas, P.M., et al., 2015. Optogenetic activation of intracellular adenosine A_{2A} receptor signaling in the hippocampus is sufficient to trigger CREB phosphorylation and impair memory. Mol. Psychiatry 20, 1339–1349.
Madeira, M.H., Boia, R., Elvas, F., et al., 2016. Selective A_{2A} receptor antagonist prevents microglia-mediated neuroinflammation and protects retinal ganglion cells from high intraocular pressure-induced transient ischemic injury. Transl. Res. 169, 112–128.
Maei, H.R., Zaslavsky, K., Teixeira, C.M., et al., 2009. What is the most sensitive measure of water maze probe test performance? Front. Integr. Neurosci. 3, 4.
Masuda, A., Kobayashi, Y., Kogo, N., et al., 2016. Cognitive deficits in single *App* knock-in mouse models. Neurobiol. Learn. Mem. 135, 73–82.
Matos, M., Augusto, E., Machado, N.J., et al., 2012. Astrocytic adenosine A_{2A} receptors control the amyloid-β peptide-induced decrease of glutamate uptake. J. Alzheimers Dis. 31, 555–567.
Matos, M., Shen, H.Y., Augusto, E., et al., 2015. Deletion of adenosine A_{2A} receptors from astrocytes disrupts glutamate homeostasis leading to psychomotor and cognitive impairment: relevance to schizophrenia. Biol. Psychiatry 78, 763–774.
Morris, R.J., 1984. Developments of a water-maze procedure for studying spatial learning in the rat. J. Neurosci. Methods 11, 47–60.
Mucke, L., Masliah, E., Yu, G.-Q., et al., 2000. High-level neuronal expression of $A\beta_{1-42}$ in wild-type human amyloid protein precursor transgenic mice: synaptotoxicity without plaque formation. J. Neurosci. 20, 4050–4058.
Muller, C.E., Geis, U., Hipp, J., et al., 1997. Synthesis and structure-activity relationships of 3,7-dimethyl-1-propargylxanthine derivatives, A_{2A}-selective adenosine receptor antagonists. J. Med. Chem. 40, 4396–4405.
Musiek, E.S., Holtzman, D.M., 2015. Three dimensions of the amyloid hypothesis: time, space and 'wingmen'. Nat. Neurosci. 18, 800–806.
Nikodijevic, O., Jacobson, K.A., Daly, J.W., 1993. Locomotor activity in mice during chronic treatment with caffeine and withdrawal. Pharmacol. Biochem. Behav. 44, 199–216.
Ning, Y.L., Yang, N., Chen, X., et al., 2013. Adenosine A2A receptor deficiency alleviates blast-induced cognitive dysfunction. J. Cereb. Blood Flow Metab. 33, 1789–1798.
Orr, A.G., Orr, A.L., Li, X.J., et al., 2009. Adenosine A_{2A} receptor mediates microglial process retraction. Nat. Neurosci. 12, 872–878.
Orr, A.G., Hsiao, E.C., Wang, M.M., et al., 2015. Astrocytic adenosine receptor A_{2A} and G_s-coupled signaling regulate memory. Nat. Neurosci. 18, 423–434.
Palop, J.J., Mucke, L., 2016. Network abnormalities and interneuron dysfunction in Alzheimer disease. Nat. Rev. Neurosci. 17, 777–792.
Palop, J.J., Chin, J., Roberson, E.D., et al., 2007. Aberrant excitatory neuronal activity and compensatory remodeling of inhibitory hippocampal circuits in mouse models of Alzheimer's disease. Neuron 55, 697–711.
Pinna, A., 2014. Adenosine A_{2A} receptor antagonists in Parkinson's disease: progress in

clinical trials from the newly approved istradefylline to drugs in early development and those already discontinued. CNS Drugs 28, 455–474.
Popoli, P., Pintor, A., Domenici, M.R., et al., 2002. Blockade of striatal adenosine A_{2A} receptor reduces, through a presynaptic mechanism, quinolinic acid-induced excitotoxicity: possible relevance to neuroprotective interventions in neurodegenerative diseases of the striatum. J. Neurosci. 22, 1967–1975.
Possin, K.L., Sanchez, P.E., Anderson-Bergman, C., et al., 2016. Cross-species translation of the Morris maze for Alzheimer's disease. J. Clin. Invest. 126, 779–783.
R Development Core Team, 2015. R: A Language and Environment for Statistical Computing. R Foundation for Statistical Computing, Vienna, Austria.
Ransom, B.R., Ransom, C.B., 2012. Astrocytes: multitalented stars of the central nervous system. Methods Mol. Biol. 814, 3–7.
Rebola, N., Simões, A.P., Canas, P.M., et al., 2011. Adenosine A_{2A} receptors control neuroinflammation and consequent hippocampal neuronal dysfunction. J. Neurochem. 117, 100–111.
Rice, J.P., Wallace, D.G., Hamilton, D.A., 2015. Lesions of the hippocampus or dorsolateral striatum disrupt distinct aspects of spatial navigation strategies based on proximal and distal information in a cued variant of the Morris water task. Behav. Brain Res. 289, 105–117.
Rissanen, E., Virta, J.R., Paavilainen, T., et al., 2013. Adenosine A2A receptors in secondary progressive multiple sclerosis: a [11C]TMSX brain PET study. J. Cereb. Blood Flow Metab. 33, 1394–1401.
Sahlin, C., Lord, A., Magnusson, K., et al., 2007. The Arctic Alzheimer mutation favors intracellular amyloid-β production by making amyloid precursor protein less available to α-secretase. J. Neurochem. 101, 854–862.
Saito, T., Matsuba, Y., Mihira, N., et al., 2014. Single App knock-in mouse models of Alzheimer's disease. Nat. Neurosci. 17, 661–663.
Schwarzschild, M.A., Agnati, L., Fuxe, K., et al., 2006. Targeting adenosine A_{2A} receptors in Parkinson's disease. Trends Neurosci. 29, 647–654.
Serrano-Pozo, A., Betensky, R.A., Frosch, M.P., et al., 2016. Plaque-associated local toxicity increases over the clinical course of Alzheimer disease. Am. J. Pathol. 186, 375–384.
Shen, H.Y., Coelho, J.E., Ohtsuka, N., et al., 2008. A critical role of the adenosine A_{2A} receptor in extrastriatal neurons in modulating psychomotor activity as revealed by opposite phenotypes of striatum and forebrain A_{2A} receptor knock-outs. J. Neurosci. 28, 2970–2975.
Shen, H.Y., Canas, P.M., Garcia-Sanz, P., et al., 2013. Adenosine A_2A receptors in striatal glutamatergic terminals and GABAergic neurons oppositely modulate psychostimulant action and DARPP-32 phosphorylation. PLoS One 8, e80902.
Tavares, A.A., Batis, J.C., Papin, C., et al., 2013. Kinetic modeling, test-retest, and dosimetry of ^{123}I-MNI-420 in humans. J. Nucl. Med. 54, 1760–1767.
Viana da Silva, S., Haberl, M.G., Zhang, P., et al., 2016. Early synaptic deficits in the APP/PS1 mouse model of Alzheimer's disease involve neuronal adenosine A_{2A} receptors. Nat. Commun. 7, 11915.
Vianna, M.R., Alonso, M., Viola, H., et al., 2000. Role of hippocampal signaling pathways in long-term memory formation of a nonassociative learning task in the rat. Learn. Mem. 7, 333–340.
Wang, J.H., Ma, Y.Y., van den Buuse, M., 2006. Improved spatial recognition memory in mice lacking adenosine A_{2A} receptors. Exp. Neurol. 199, 438–445.
Wei, C.J., Singer, P., Coelho, J., et al., 2011. Selective inactivation of adenosine A_{2A} receptors in striatal neurons enhances working memory and reversal learning. Learn. Mem. 18, 459–474.
Yang, M., Soohoo, D., Soelaiman, S., et al., 2007. Characterization of the potency, selectivity, and pharmacokinetic profile for six adenosine A_{2A} receptor antagonists. Naunyn Schmiedeberg's Arch. Pharmacol. 375, 133–144.
Yu, L., Shen, H.Y., Coelho, J.E., et al., 2008. Adenosine A_{2A} receptor antagonists exert motor and neuroprotective effects by distinct cellular mechanisms. Ann. Neurol. 63, 338–346.
Zhang, B., Gaiteri, C., Bodea, L.G., et al., 2013. Integrated systems approach identifies genetic nodes and networks in late-onset Alzheimer's disease. Cell 153, 707–720.